IMAGING CHARGE-COUPLED DEVICE (CCD) TRANSIENT RESPONSE TO 17 AND 50 MEV PROTON AND HEAVY-ION IRRADIATION

T. S. Lomheim, R.M. Shima, J.R. Angione, W.F. Woodward,
D.J. Asman, R.A. Keller, and L.W. Schumann
The Aerospace Corporation
Optical Systems Department
P.O. Box 92957
Los Angeles, CA 90009-2957

ABSTRACT

We report the results of irradiating a high-resolution, large-area, silicon charge-coupled device (CCD) imaging array (Kodak KAF-1400) with controlled low fluxes of collimated monoenergetic (17 and 50 MeV) protons and selected heavy ions. We measured the CCD response at several angles-of-incidence, from normal to 70° off normal and at several azimuthal angles. The transient response events were recorded and analyzed to infer the effective charge collection depth of the CCD. We analyzed selected individual proton-induced events for their two-dimensional spatial amplitude and compared the results to a charge collection model which included contributions from both the pixel depletion and diffusion volumes for the geometry (pixel size and spacing) and thicknesses (depletion depth and epitaxial layer thickness) of this CCD.

I. INTRODUCTION

Space-based systems employing area or linear charge-coupled device (CCD) arrays are potentially susceptible to transient radiation effects, such as those induced by ionizing particles (e.g. protons, heavy-ions) passing through the charge-collection volume of the CCD detecting elements (pixels)[1]. Protons are of concern in low-to-medium earth orbits because the South Atlantic (geomagnetic) anomaly permits high fluxes of energetic protons[2] to penetrate to low altitudes. Ionization-induced charges in the CCD array appear as unwanted signals in the video data.

When the proton induced events compete with the CCD signals, detectivity is degraded due to an increase in the rate of false alarms. Mitigation techniques might include: a) reducing the system sensitivity by gating the system off during occasions of high proton flux, b) applying signal processing techniques to reject the transient events, or c) designing the CCD structure to be less susceptible to ionizing radiation.

While increasing the detection threshold might be practical in some space applications, reduced sensitivity is generally unacceptable. One signal processing technique which works at relatively low proton flux is to differentiate the targets, which persist from frame-to-frame, from the proton events which occupy only a single frame. At higher fluxes, more sophisticated processing is required based on systematic differences between the spatial and amplitude characteristics of the signal and unwanted proton events. In principle you can reduce the sensitivity of the CCD to ionizing radiation by reducing the pixel volume, by reducing the depletion and diffusion depth, but this will reduce the detector responsivity at longer wavelengths. Our experiment is generally relevant to the recent SEU work performed by Zoutendyk et al.[3,4] on static and dynamic random-access memories (SRAM and DRAM). The so-called SEU induced error "bit-maps" and the ability to infer active collection thicknesses are analogous to some of the results of this work except that the SRAM and DRAM devices are digital, giving responses that are equivalent to zero or one; the CCD is an analog device where the measurement of collected charge at each pixel site to a high amplitude resolution is possible.

We report the results of irradiating a high-resolution, large-area, commercial, visible silicon CCD imaging array[5] with controlled low fluxes of collimated monoenergetic (17 and 50 MeV) proton and selected heavy-ions. The charged-particles were incident at angles ranging from normal to 70° off-normal and at several azimuthal angles. The experimental results were compared to a relatively simple solid state model of a CCD array and the generally good agreement between analysis and observation validated this model. With this validated model we are now confident that we can quantitatively predict the transient response of a CCD array in a space sensor application to charged particle environments, provided the CCD design and architecture, sensor shielding, and particle environment are known.

II. EXPERIMENTAL DETAILS

The charged-particle irradiation experiments were carried out using the 88-in. sector-focussed cyclotron of the Lawrence Berkeley Laboratory. The charged-particles used are listed in Table 1 including their charge state, nominal energy, range and linear-energy-transfer (LET) in silicon at this nominal energy[6]. The latter is also listed in units of electron-hole pairs (EHP) per unit length (μm) for convenience in the subsequent interpretation of the data.

Table 1. Charged Particles Used in Irradiation Experiments

Charged Particle (charge-state)	Energy (MeV)	LET (MeV cm²/mg)	LET (EHP/μm)	Range (μm)
Proton (1+)	50	0.010	6.40×10^2	1.2×10^4
Proton (2+)	17	0.024	1.54×10^3	1800
Nitrogen (3+)	95	2.4	1.50×10^5	120
Neon (4+)	90	5.7	3.60×10^5	54
Argon (8+)	180	14.9	9.50×10^5	47
Krypton (17+)	378	39.3	2.50×10^6	44

Note that only two energies for protons are listed; changing proton energy required the multi-hour procedure of re-tuning the cyclotron.

0018-9499/90/1200-1876$01.00 © 1990 IEEE

Figure 1 displays the charged-particle beam-to-CCD irradiation geometry and defines the specific values for the angles-of-incidence (θ) and azimuth angles (ϕ) used in the experiment. Figure 2 is a block diagram of the experimental system. The vacuum test chamber was necessary both because the CCD array required cooling to about -30°C (accomplished with a thermoelectric cooler and water heat exchanger), and the proton and heavy-ion beam transport required a moderate vacuum to minimize scattering. The CCD device was mounted on a two-axis rotational mount that permitted the range of incidence and azimuth angles indicated in Fig. 1. The rotational mount was built using stepper-motor-activated optical mounts; this mechanism along with the water heat exchanger were all placed inside the vacuum chamber. Rather than build a complex electrical interface for the rotational mount, a video camera was installed above the test chamber (which had a transparent plexiglass lid) along with a remotely controlled light source. The latter, when turned-on, illuminated the inside of the test chamber including two carefully delineated scales from which incidence and azimuth angles could be directly read. The video observation of the remote rotational mount manipulation was an essential cross-check on correct test chamber operation.

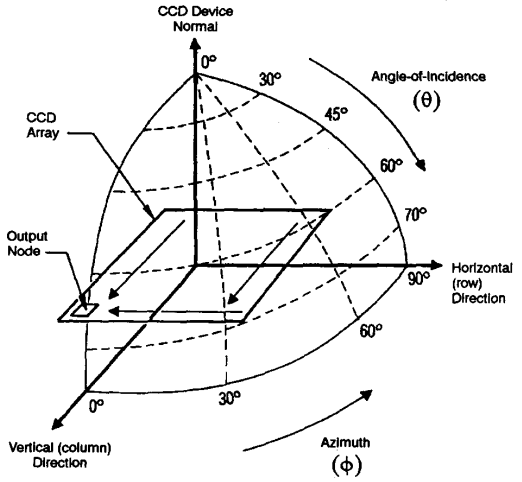

Figure 1. Definition of charged-particle geometry used for CCD irradiation

The analog wide-band clocks and the d.c. bias control signals necessary to operate and multiplex the CCD device [5], and the control lines needed to manipulate the rotational mount, were routed into the vacuum chamber via vacuum electrical feedthroughs including a co-axially shielded low-noise wide-bandwidth video line for the CCD output. The cooling water lines needed for the internal heat exchanger were also routed into the vacuum chamber via special feedthroughs. The CCD device and rotational mount in the chamber, device cooling system and heat exchanger, CCD drive, signal processing and control electronics, line drivers, remote camera and light source, were all located inside an enclosed vault area where the charged-particle beams were routed. The video analog-to-digital converter (ADC), the 386-based computer, the high-speed direct-memory-access (DMA) data capture memory, image processing system, display monitors, and digital data storage systems were located outside this vault. The 560 kHz serial video analog CCD signal propagated a distance of about 30 feet outside the vault to the ADC. A set of interlinked software subroutines were appropriately executed in the 386 computer under control of a main program for carrying out the necessary sequences needed to run the experiment.

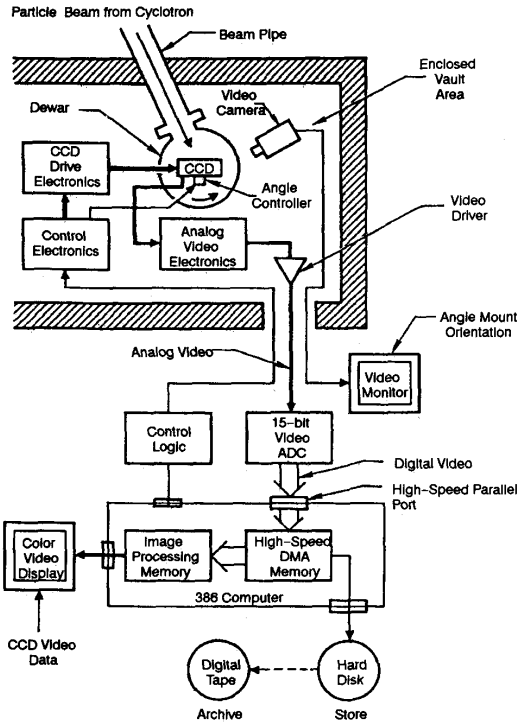

Figure 2. Block diagram of experimental arrangement used for CCD data collection during charged-particle irradiation

The CCD array was continuously operated as it was irradiated with a given charged-particle beam. The ionization-induced charge patterns collected at the pixel sites were clocked in parallel to the on-chip serial CCD shift register which fed a single on-chip electrometer that performed charge-to-voltage conversion. The CCD's single video time-division multiplexed output consists of a stream of voltage steps, where the amplitude of each step represents the signal charge collected at a pixel. The entire array of 1035 (vertical) by 1320 (horizontal) pixels was clocked out in 2.55 s. The 1035 vertical lines were clocked in parallel at a rate of 406 lines/s (2.46 ms/line) to a single 1320 pixel on-chip serial CCD multiplexer which was operated at a rate of 560,000 pixels/s (1.79 μs/pixel), which allowed 60 overscan pixels to be included in each line. The low frame rate necessitated the cooling of the device to -30°C to avoid shot

noise produced by dark current and thereby preserve the 45 rms electron/pixel noise floor. The analog amplitude dynamic range of the CCD was about 1000-to-1, from the noise floor of 45 rms electrons/pixel to the pixel saturation level of about 50,000 electrons/pixel.

The video stream was amplified, processed for noise reduction using correlated-double sampling, and then routed to the 15-bit ADC via a video line driver. The digitized version of the video stream (now 15-bits per pixel including a voltage offset) was captured in a high-speed memory board located in an Intel 386-based computer using DMA. The memory was sized to capture half of a full 1035 by 1380 (1320 plus 60 pixels of overscan) frame although the desired half-frame (1.4 Mbytes at 2 bytes/pixel) could be selected before capture. The digitized half-frame was accessible by FORTRAN-callable routines for loading into a 2D FORTRAN array for subsequent mathematical processing. We also used a 386-based image processing system for data display. This system consisted of an image processing board (which plugged into the 386 computer) and a stand-alone software package that allowed image-manipulation functions (image zoom and pan, contrast-stretch, etc.). The captured video half-frame was reformatted and loaded into the image processing board at high speed via an optimized machine language program. The time required to capture a frame of data and display it on this system was about 10s. Finally the video half-frame could be stored to hard-disk (this required 45s) and data archiving and back-up were done with a digital tape unit.

III. RESULTS: STATISTICAL SUMMARY

The CCD is a two-dimensional array of 1035 by 1320 elements (or pixels) each 6.8 by 6.8 μm [5]. Figure 3(a), which is taken from Ref. 7, shows planar and cross sectional views of four adjacent pixels of the device. The active charge collection region of the device consists of the epitaxial p-doped layer shown. The so called "p-epi" layer is epitaxially grown on a very heavily doped p-substrate and has a design thickness of 15 μm. Figure 3(b) shows pixel-gate-voltage-induced potential contours as a function of depth beneath a pixel[8]. The contours extend to a depth of 3 μm and the associated electric field causes separation of electrons and holes; the electrons (minority carriers in the p-epi layer) are attracted toward the overlying pixel and collected, the holes repelled into the diffusion layer where they recombine. This 3 μm layer is referred to as the depletion layer. Below a depth of 3 μm the potential lines do not depend on the overlying gate biases. This field free region, the diffusion layer, extends from 3 μm through the remaining effective depth of the p-epi layer. Charge generated below the p-epi layer in the heavily doped substrate quickly recombines and hence is not available for collection. However, charge generated in the diffusion layer can migrate to several adjacent pixels and, upon passing the diffusion-to-depletion layer boundary at a particular pixel, be collected by that pixel. Note that the minority-carrier (electron) diffusion length is many times the diffusion layer depth. The p-epi-to-substrate interface is not a sharp boundary as a result of the CCD processing, hence, the p-epi layer thickness is an effective thickness. Proton or heavy-ion generated minority carriers (electrons) are collected at each pixel site from the ionization produced by the passage of charged-particles through the depletion and diffusion layers.

A. RESPONSE TO PROTONS

For proton-induced events, we assume that the incident proton continues in a straight-line trajectory through the charge collection volume of the CCD. The protons are so energetic (> 17 MeV) that their range is much greater than the longest trajectory through the epi-layer; thus we can assume a constant LET of EHP generation rate along their trajectory. For the largest incidence angles used ($\theta = 70°$), the maximum trajectory length in the CCD active layer was 15 μm X secant(70°) or 44 μm. At 3.62 eV (electron volts) per EHP and an LET of 1540 EHP/μm for a 17 MeV proton, only 0.24 MeV in energy is given up along this trajectory length. This fractional loss is even less at 50 MeV. The 17 and 50 MeV proton ranges (Table 1) in silicon greatly exceed the maximum 44 μm effective charge collection length in the p-epi layer.

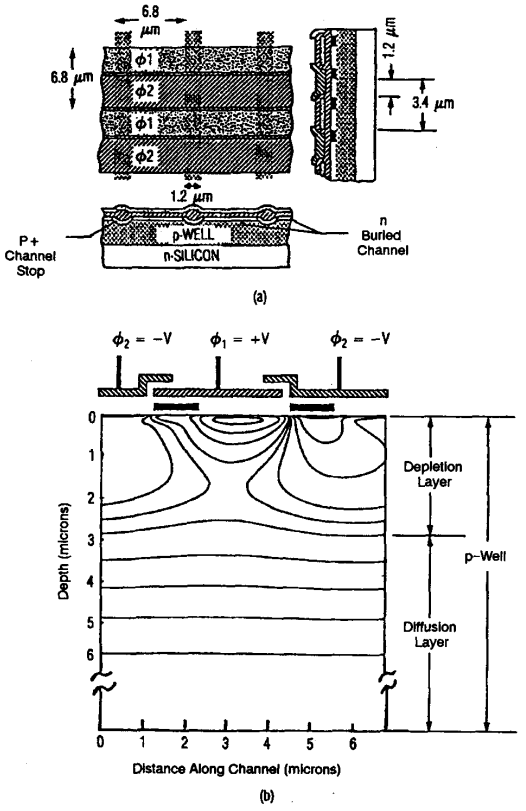

Figure 3. (a) Planar and cross-sectional views of pixel area for CCD sensor. (b) Potential contour beneath two-phase gates of single CCD pixel.

Figures 4 through 7 show the CCD responses, in a 250 by 250 pixel area of the video output, to 17 MeV protons as a function of different incidence and azimuth angles (θ and ϕ respectively in Figs. 4 through 7) at a low and relatively constant flux. In Fig. 4 ($\theta = 0°$ and $\phi = 0°$) about 100 events, each covering a few pixels (2 or 3 pixels in each direction), are visible. This corresponds to normally incident irradiation and no particular symmetry is evident for the events. These events look somewhat similar to those produced by irradiating a CCD with x-rays (see Fig. 2 of Ref. [9]), however the basic mechanism for charge generation by x-rays is different than for charged-particle irradiation. Figures 4 through 7 have been highly contrasted to make the events clearly observable with the result that the detail of the amplitude distribution across individual events is lost. See Section IV for the analysis of selected individual event amplitude profiles. In Fig. 5, ($\phi = 0°$, $\theta = 70°$) the beam enters the CCD at 70° to the normal but is aligned with the pixel rows (horizontal axis). Here the events are elongated in the row (horizontal) direction compared to the column (vertical) direction. The large angle of incidence results in a longer trajectory through the device charge-collection layers, one that corresponds to traversing beneath several pixels before descending into the heavily doped substrate. Figure 6 ($\phi = 30°$, $\theta = 70°$) shows the same general features as Fig. 5 since they both correspond to the same incidence angle, however, the event elongation is along the 30° azimuth direction as indicated. In Fig. 7 ($\phi = 60°$, $\theta = 70°$) the direction is rotated still further with the elongation along the 60° azimuth.

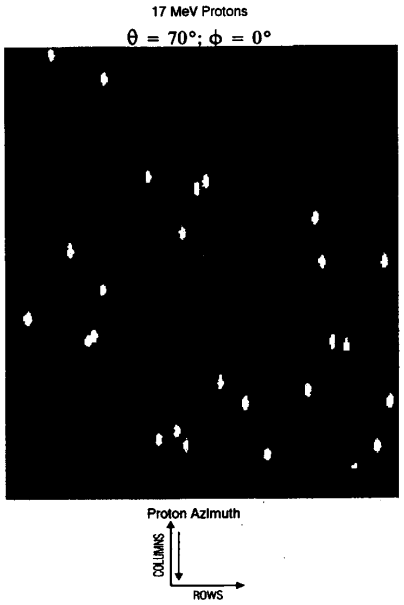

Figure 5. CCD video response; 17 MeV protons, $\theta = 70°$, $\phi = 0°$.

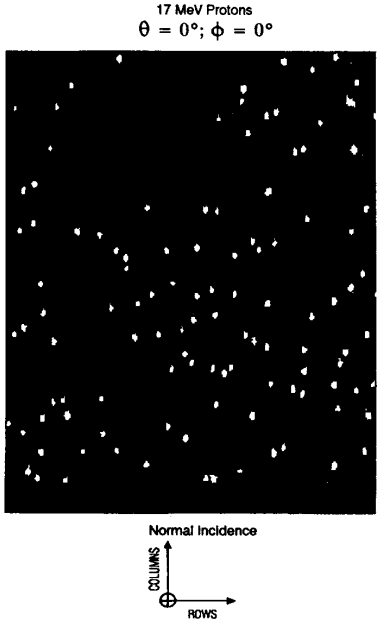

Figure 4. CCD video response; 17 MeV protons, $\theta = 0°$, $\phi = 0°$.

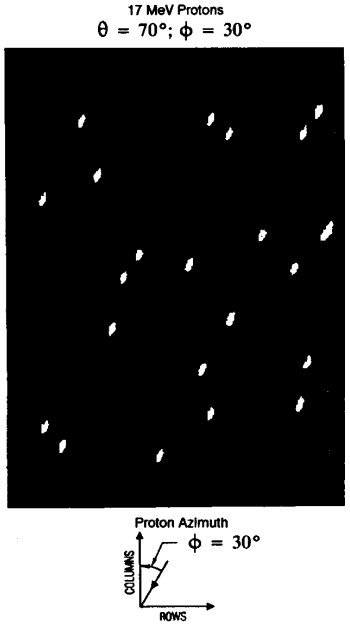

Figure 6. CCD video response; 17 MeV protons, $\theta = 70°$, $\phi = 30°$.

Figure 7. CCD video response; 17 MeV protons, $\theta = 70°$, $\phi = 60°$.

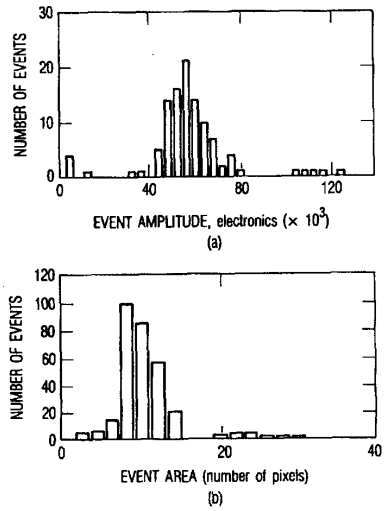

Figure 8. Histograms for 17 MeV protons, $\theta = 70°$, $\phi = 0°$ (a) Event amplitude, (b) Event spatial area

Variations in specific proton trajectories, and CCD charge collection effects, as well as scattering, contribute to the distribution in both the extent and total charge generated from event-to-event, for a given beam energy and incidence/azimuth angle set. Figures 8(a) and 8(b) are histograms, showing the effect of these variations for the specific case of 17 MeV protons incident at $\theta = 70°$ and $\phi = 0°$. In Fig. 8(a) the amplitude distribution of the individual proton-response events has a mean of about 55,000 electrons and a standard deviation of about 20% of the mean. Similarly, Fig. 8(b) shows the distribution of the individual event areas given as the total number of pixels each event covered. For this case the average event covered about 10 pixels, consistent with the typical event area extent shown in Fig. 5. The histograms were obtained by exercising a computer program that associated clusters of adjacent pixels, which stood above a predetermined threshold level, as transient events. Once a cluster was deemed an event, its total charge and area were computed. An entire frame of data was analyzed automatically this way. The program only worked reliably for data frames with fairly sparse events; some of the frames with high event densities had to be analyzed by hand (using far fewer events).

The particle trajectory length through the active layers in the CCD scales as the secant of the angle-of-incidence (θ) per Fig. 1. This implies that the total collected charge per event should also scale as secant (θ), independent of the azimuthal angle. Figure 9(a) is a plot of the mean event charge versus secant (θ), for various azimuth angles and 17 MeV protons. The error bars correspond to $\pm$ one standard deviation in the data used for each point. The first data point corresponds to the case of normal incidence where the collected charge is due to the proton track along the minimum possible trajectory length, the device active layer thickness. The straight line in Fig. 9(a) is extended through zero since an infinitely thin active layer would collect no charge. Accordingly, the straight line represents a fit to the data, with the constraint that it pass through the origin. Dividing the mean event charge from Fig. 9(a) by the EHP generation rate of $1.54 \times 10^3/\mu m$ (Table 1) and the cos(θ) results in an apparent carrier collection depth of 10.8 μm, which compares favorably to the nominal p-epi layer design thickness of 15 μm [Fig. 3(b)]. Figure 9(b) shows the mean event charge for 50 MeV protons. In this case we see the data drops off for $\theta < 45°$. The combination of this relatively high proton energy and these shorter trajectory lengths makes the induced events rather small. In a given event the diffusion component of the signal charge is spread over many pixels making it more difficult to estimate at low signal to noise ratios. Consequently two lines are shown in Fig. 9(b), one using all the data, the other using only the data for $\theta > 60°$. In both cases the lines are constrained to pass through the origin. The upper line gives an effective layer thickness of 10.4 μm and the lower line 9.11 μm, assuming an LET of 640 EHP/μm for 50 MeV protons. With the indicated discrepancy of the short trajectory data, this is consistent with the results obtained for the 17 MeV proton irradiation.

The above results indicate that the magnitude of the proton-induced events scale in an expected manner with incidence angle (e.g. trajectory length through the CCD charge collection layer) and energy and that all of the charge generated in the volume associated with this layer by a passing energetic proton is collected by the affected adjacent CCD pixels.

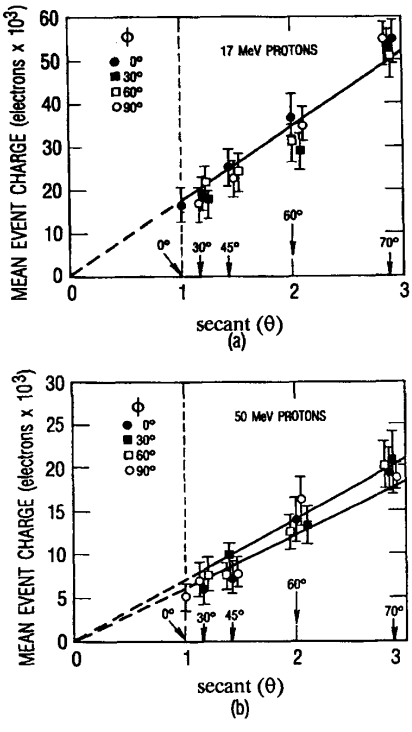

Figure 9. Mean proton-induced event charge versus secant(θ) (a) 17 MeV protons; inferred layer thickness = 10.8 μm. (b) 17 Mev protons; inferred layer thickness = 9.1 to 10.4 μm

B. RESPONSE TO HEAVY-IONS

The CCD was also irradiated with four heavy-ions of increasing LET as indicated in Table 1. From right-to-left in Fig. 10 we see that the unusual CCD video responses increase in area with increasing LET. These shapes result because charge overflows from the pixel impacted by the ion into adjacent pixels. The number of carriers created over even the shortest trajectory easily exceeds the 50,000 electron/pixel saturation limit of this CCD. The saturation overflow is clearly very asymmetric, with the vertical direction being the preferred direction for the overflow. This overflow occurs against the direction of the CCD charge transport and is due to the nature and clocking of the 2-phase vertical CCD gates.* Note that while the saturation phemonena obliterate the spatial structure of the heavy-ion induced event, the total generated charge is not lost, but rather is collected by the affected pixels. Figure 11(a) is a plot of the mean collected charge per heavy-ion event versus the LET for the corresponding heavy-ion, for the four ions at $\theta = 0°$ and 70°. For $\theta = 0°$ the charge collected is directly proportional to the LET and dividing the charge by the LET results in an estimated collection depth of 13.6 μm. The $\theta = 70°$ case shows a decrease in collected charge with increasing LET. The straight line was obtained by multiplying the $\theta = 0°$ line by the secant (θ) factor of 2.92. The lower LET points fit this line while the higher LET points do not.

For the grazing incidence particle, i.e., $\theta = 70°$, the range of the heavy-ions relative to the distance traveled in the charge-collection layer must be considered. The projected ranges of the heavy-ions are: nitrogen(3+) = 120 μm, neon(4+) = 53 μm, argon(8+) = 46 μm, and krypton(17+) = 43 μm. These ranges were computed** after reducing the incident energies by the loss in passing through 2 μm X secant (70°) = 6 μm of thermally-deposited overlying glass which is used as a scratch-protection covering for the CCD, and hence are slightly shorter than those listed in Table 1. For normal incidence this energy loss in the glass over-layer can be neglected.

For normally incident heavy-ion range is much greater than the maximum charge-collection (p-epi layer) thickness of 15 μm, but at $\theta = 70°$ both krypton(17+) and argon(8+) stop inside the charge collection depth and neon(4+) stops just outside. The assumption of a constant LET along the trajectory length is clearly not met for these cases.

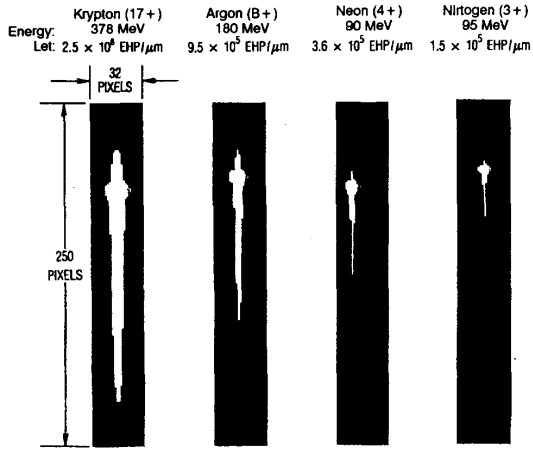

Figure 10. CCD video response to the heavy ions N(3+), Ne(4+), Ar(8+), and Kr(17+).

IV. PROTON SINGLE-EVENT ANALYSIS AND MODELLING

Understanding the details of the spatial shapes and magnitudes of the individual events requires developing a model for predicting these characteristics. To this end we developed a simple model that requires as inputs: the proton kinematics (θ, ϕ and energy), an assumed (x,y) entry point into the CCD, the CCD depletion and diffusion layer thicknesses, and the dimensions of a pixel along with the associated CCD pixel surface

*T. H. Lee and W. C. Chang, Eastman-Kodak, private communication.

**Computed using the computer program TRIM-89 by J.P Biersack and J.F. Ziegler.

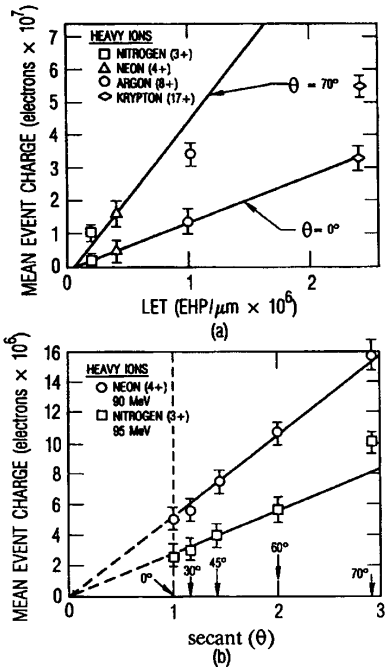

Figure 11 (a) Mean particle-induced event charge versus LET for four heavy-ions (N, Ne, Ar, Kr); inferred layer thickness = 13.6 μm. b) Mean particle-induced event charge versus secant(θ) inferred layer thickness = 17.8 μm for Nitrogen, 14.8 μm for Neon.

topology. Figure 12 shows a proton incident on a pair of adjacent pixels. The pixel structure is replicated in the x and y directions to form a two-dimensional array of pixels. The proton, following a straight line trajectory, enters pixel 1 at position $P_0 = (x_0,y_0,0)$, where the origin is defined at the upper left-hand vertex of this pixel. The trajectory of the proton is defined by the conventional spherical coordinates shown in Fig. 12. The proton passes into pixel 2 at position $P_1 = (x_1,y_1,z_1)$ where clearly $y_1 = d$. Finally the proton passes out of the bottom of pixel 2 $P_2 = (x_2,y_2,z_2)$ where $z_2 = z_{depl}$. From positions P_0 to P_2 the proton trajectory is in the depletion layer of the CCD, first under pixel 1 and then under pixel 2. The electric fields present in the depletion volume under a given pixel collect any charged-particle-induced minority carriers (electrons) produced in that pixel volume. If we know the particle trajectory through one or more adjacent pixel depletion volumes, we can determine the charge collected by each pixel by multiplying the particle trajectory length in each pixel by the LET. For example, in Fig. 12 the total depletion charge collected by pixel 1 would be the distance from P_0 to P_1 times the LET, for pixel 2 it would be the distance from P_1 to P_2 times the LET. The number of pixel depletion volumes crossed depend on the particle kinematics; for large angles-of-incidence, more pixels would generally be crossed than for small angles-of-incidence. Once the charged-particle descends below the depth

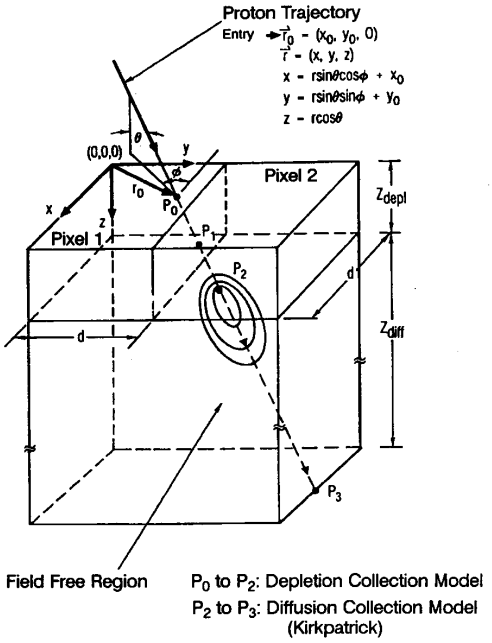

Figure 12 Schematic showing proton trajectory through depletion and diffusion volumes of two adjacent pixels.

corresponding to the depletion layer ($z = z_{depl}$ in Figure 12), the diffusion volume of the CCD is entered. The model for depletion layer charge collection amounts to nothing more than computing line segment lengths though adjacent parallelepipeds (pixel depletion volumes) given an entry point and trajectory definition. Note that this computation is similar to that used by Pickel and Blandford[10] in evaluating heavy-ion induced SEU's in MOS memories.

To compute the charge collected from the diffusion layer(shown as the dimension z_{diff} in Figure 12) we apply a simple model taken from Kirkpatrick[11]. In the diffusion volume there are no electric fields, hence, ionization-induced charge diffuses to adjacent pixels. The Kirkpatrick model starts by solving the 3-dimensional diffusion equation in a field-free semi-infinite medium assuming a point source due to EHP generation (units of EHP/volume) at some depth into the diffusion region. (The effects of recombination are neglected at this stage of the model but are later included using an approximation.) The method of images is then used to establish boundary conditions for the point-source solution. The resulting current density at the depletion-diffusion layer boundary interface (the plane given by $z = z_{depl}$ in Fig. 12) is computed by taking the negative of the diffusion coefficient times the normal gradient of the point source density evaluated at the interface. That the normal gradient is used, assumes that the interface is a perfect absorber. This current density is integrated over the device integration period, which is considered infinite for mathematical simplicity. The CCD parallel line time of 2.46 ms is much longer (for our clocking rates)

than the time required for charge to diffuse to the surface for collection, hence this approximation is justified. This gives the charge per unit area at the depletion-diffusion layer interface obtained from a point-source inside the diffusion region. This method is then generalized to a line of EHP's representing the ionization track of a charged particle corresponding to the trajectory from points P_2 to P_3 in Fig. 12. The final steps in the model consist of: (a) integrating down this line (from P_2 to P_3) where the chosen length determines the effective diffusion layer thickness of the device (denoted z_{diff}), herein approximating the effects of recombination and, (b) integrating over the pixel areas at the diffusion-depletion layer boundary. The entire model was assembled by first computing the depletion charge generated from P_0 to P_2 and then using the point P_2 as the entry point for the diffusion charge calculation and finally adding the two resulting (depletion and diffusion) pixel maps together.

To test this model, several 17 MeV proton events were examined. The comparison between these experimental observations and the model predictions are shown in Figs. 13-16. The parameters used in this model were those of the Kodak CCD: 6.8 by 6.8 μm pixel with a 6.8 μm pitch, a 3 μm depletion depth, and an 8 μm diffusion depth. Note that the depletion plus diffusion width is essentially the value inferred from the slope of Fig. 9(a) based on analyzing the total charge collected. Figures 13 and 14 show the case of normal incidence ($\theta = 0°, \phi = 0°$). In Figs. 13(a) and 13(b), contour plots of constant collected charge versus pixel position are shown for an area of about 20 by 20 μm (3 by 3 pixels) for the experimental event and modelled event, respectively. The pixel responses (in electrons/pixel) are log scaled in this figure. Note that the proton did not enter in the center of a pixel as indicated by the slight asymmetry in the contour plots. Figures 14(a) and 14(b) show x and y direction semi-log profile plots of this event, again for the experimentally observed event and the modelled event, respectively. Good qualitative agreement is seen between the experimental and modelled events where both have about the same peak signal amplitude. The total integrated charge in the experimental and modelled events agreed to within a few percent using a threshold for both of 200 electrons. Given the amplitude distribution in the observed events in even one frame, there was clearly a variety of different amplitude experimental events from which to choose. The event integrated amplitude corresponded to a level very close to the center of the data point shown on Fig. 9(a) for $\theta = 0°$. Hence "typical" events matched well with the model. This approach to experimental versus modelled event matching was also employed for the two examples discussed below.

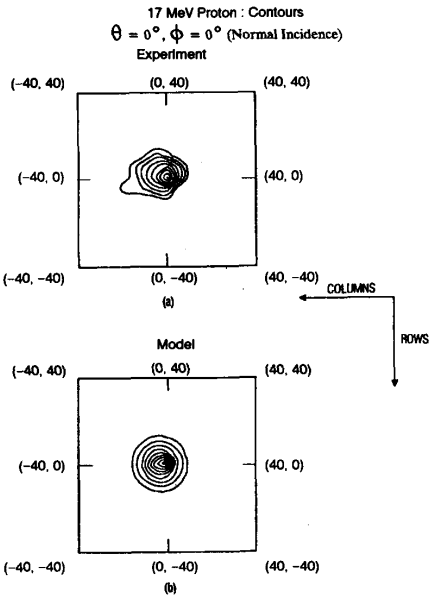

Figure 13 Contour plot showing a proton-induced-event-amplitude versus pixel position for a 40 by 40 block of pixels for 17 MeV protons at normal incidence. Amplitudes are log-scaled. (a) Experiment, (b) Model

Figures 15 and 16 show experimental and modelled responses for 17 MeV protons with trajectories of $\theta = 70°$ and $\phi = 0°$. This means the protons were travelling parallel to the CCD column direction. Here the contour plots of Fig. 15 clearly show a large asymmetry in the column direction as would be expected. This asymmetry is better seen in the profile plots in Figs. 16(a) and 16(b). Note that the qualitative match between the experimental and modelled events is good. However, the modelled event appears to spread-out more than the observed event. The total integrated charge in the experimental event fell within the experimental uncertainty of the inferred charge collection depth. Obtaining a good match for this case required exercising the model for different proton entry positions (point P_0 in Fig. 12). Clearly we have no a priori knowledge of a proton's entry position on a CCD pixel and hence model iterations for various trial entry positions were necessary. Finally, the role of the depletion component of the charge pattern should be appreciated. Figure 16(b) shows profile plots where in the x-direction, the highest two amplitude pixels stand out well above the adjacent pixels because of this depletion layer contribution. At $\theta = 70°$, the incident proton enters and traverses the depletion volumes of these two pixels and then descends into the diffusion volume. Clearly the highest amplitude pixel of these two experiences the longest proton trajectory length.

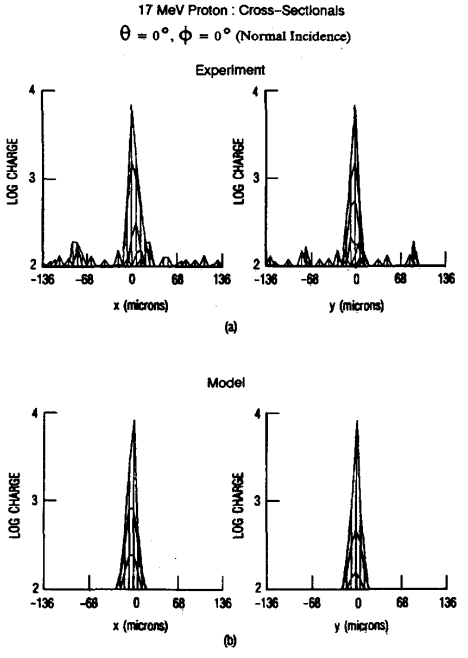

Figure 14 Cross-section plots of a proton-induced event for 17 MeV protons at normal incidence. (a) Experiment, (b) Model

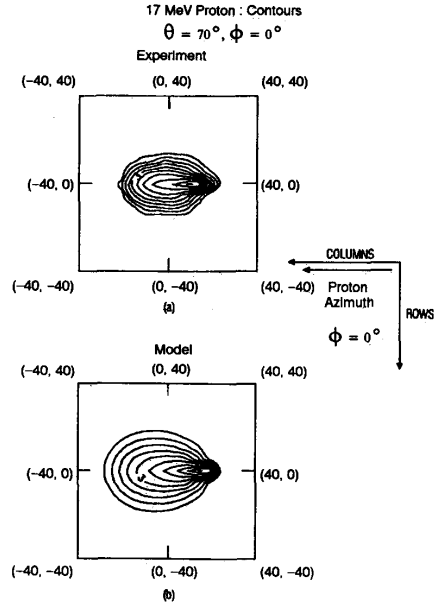

Figure 15 Contour plot showing a proton-induced-event-amplitude versus pixel position for a 40 by 40 block of pixels for 17 MeV protons and θ = 70°, ϕ = 0°. Amplitudes are log-scaled. (a) Experiment, (b) Model

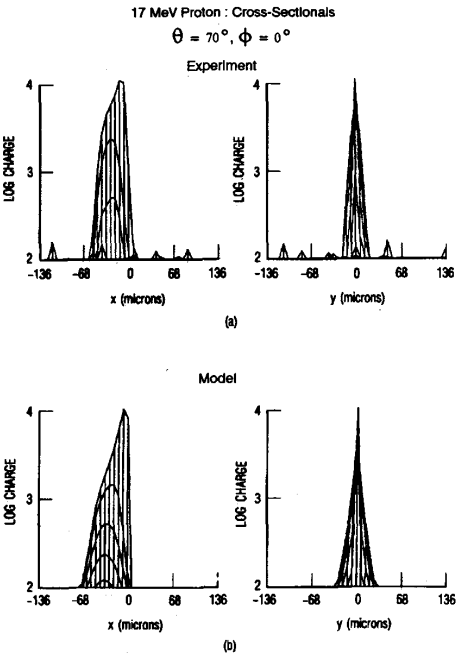

Figure 16 Cross-section plots of a proton-induced event for 17 MeV protons and θ = 70°, ϕ = 0° (a) Experiment, (b) Model

V. CONCLUSIONS

The results of this investigation provided considerable insight into the statistical and physical nature of proton and heavy-ion induced transient responses in a large area CCD imaging array of known architecture and design. The results of the statistical analysis of the charged-particle response data support the idea that all of the ionization-induced charge generated within some charge-collecting layer (depletion plus effective diffusion layer thicknesses) of the CCD are collected and counted as events. This inferred thickness was fairly close to the CCD's p-epi layer design thickness of 15 μm which represents the maximum charge collection layer thickness possible for optically induced charge collection. Specifically, the 17 and 50 MeV proton irradiation data pointed toward a charge-collection layer thickness of between 10 and 11 μm, while the heavy-ion data implied a charge-collection layer thickness in the 14 to 17 μm range. Based on the error-bars in Fig. 9, we do not consider these differences to be statistically significant. There was evidence that for the two most massive heavy-ions at large angle cases (θ = 70°) the ion range was less than the trajectory length through the charge-collection layer.

The model predictions matched several experimental observations within 20%. The key difference was that the model tended to spread the charge collection volume out more than was observed. The model included both depletion and diffusion volumes, although it appears the diffusion volume was not modelled

precisely. The role of the depletion and diffusion components of the collected charge stood out in both the experimental and modelled events; the impact of an improved diffusion model will be investigated. The results of this investigation indicate that a predictive single event model can be used to fairly accurately assess the impact of proton- induced transient responses in CCD imagers, where the nominal device architecture parameters are known. It would be interesting to irradiate a series of high-resolution CCD area arrays of increasing p-epi layer thickness to investigate the effect of increasing the diffusion component of the ionization-induced charge, and test the ability of the model to predict the resulting event shapes. Small pixels would be needed to provide good spatial resolution of the observed events; however, such a series of CCD's would probably have to be specially fabricated as research devices since their utility as optical imaging arrays would be limited in most applications. The results of this work also provide some basis for optimizing CCD designs for reduced transient response to charged-particles, for example by reducing the active layer thicknesses. This, however, must be done without unacceptably degrading the desired CCD optical performance.

VI. ACKNOWLEDGMENTS

This work was supported by The Aerospace Corporation company sponsored-research funds. We wish to thank Professor J.Choma, Jr. for his unending enthusiastic support, and P. J. Peters, R. B. Schoolar, and S. Hovanessian for their careful review of the manuscript. We also thank R. Koga and W. A. Kolasinski for helpful suggestions on the operation of particle accelerators, and gratefully acknowledge the expert assistance of L. Chlosta, G. Low, an R.M. Larimer of the Lawrence-Berkeley 88-in. cyclotron staff.

VII. REFERENCES

[1] S. Marcus, R. Nelson, and R. Lynds, "Preliminary Evaluation of a Fairchild CCD-211 and a New Camera System," *Proc. of the SPIE*, Vol. 76, pp. 207-231, 1979.

[2] E.G. Stassinopoulos and J. P. Raymond, "The Space Radiation Environment for Electronics", *Proc. of the IEEE*, Vol. 76, pp. 1423-1442, 1988.

[3] J. A. Zoutendyk, H. R. Schwartz, and L.R. Nevill, "Lateral Charge Transport from Heavy-Ion Tracks in Integrated Circuits", *IEEE Tans. on Nucl. Sci.*, Vol. NS-35, pp.1644-1647, 1988.

[4] J. A. Zoutendyk, L.D. Edmonds, and L.S. Smith, "Characterization of Multiple-Bit Errors from Single-Ion Tracks in Intergrated Circuits", *IEEE Trans. on Nucl. Sci.*, Vol. NS-36, pp. 2267-2274, 1989.

[5] KAF-1400 1035 by 1380 "Megapixel" CCD Sensor, Specification and Data Sheet, Eastman-Kodak Company, Rochester, New York.

[6] J.F. Ziegler, J. Biersack, and U. Littmark, *The Stopping and Range of Ions in Solids*, Pergammon, New York, 1985.

[7] E.G. Stevens, T.H. Lee, D.N. Nichols, C.N. Anagostopoulous, B.C. Burkey, W.C. Chang, T.M. Kelley, R.P. Kholsa, D.L. Losee, T.J. Tredwell, "A 1.4 - Million Element CCD Image Sensor", *IEEE ISSCC Tech. Digest*, pp.114-116, 1987.

[8] D. N. Nichols, W. C. Chang, B. C. Burkey, E. G. Stevens, E. A. Trabka, D. L. Losee, T. J. Tredwell, C. V. Stancampiano, T. M. Kelly, R. P. Kholsa, and T. H. Lee, "A 1.4 Million Element Full Frame CCD Image Sensor with Vertical Overflow Drain for Anti-Blooming and Low Color Crosstalk", *IDEM Tech. Digest*, pp. 120-123, 1987.

[9] R.A. Stern, K. Liewer, and J.R. Janesick, "Evaluation of a Virtual Phase Charge-Coupled Device as an Imaging X-Ray Spectrometer", *Rev. Sci. Instrum.*, Vol. 54, pp. 198-205, 1983.

[10] J.C. Pickel and J.T. Blandford, "Cosmic Ray Induced Errors in MOS Memory Cells", *IEEE Trans. on Nucl. Sci.*, Vol. NS-25, pp. 1166-1171, 1978.

[11] S. Kirkpatrick, "Modeling Diffusion and Collection of Charge from Ionizing Radiation in Silicon Devices", *IEEE Trans. on Electr. Devices*, Vol. ED-26, pp.1742-1753, 1979.